Vlasov simulation of amplitude-modulated Langmuir waves

Takayuki Umeda[a)]
Solar-Terrestrial Environment Laboratory, Nagoya University, Nagoya, Aichi 464-8601, Japan

(Received 27 June 2006; accepted 11 August 2006; published online 11 September 2006)

Mechanisms for the generation of Langmuir wave packets are studied by performing a one-dimensional electrostatic Vlasov simulation. The present simulation of a weak-electron-beam instability without ion dynamics suggests two new processes for the amplitude modulation of Langmuir waves. The beam instability excites Langmuir modes over a wide wave number range, but the saturation of the most unstable Langmuir mode "filters" the growth of sideband modes. Specific upper and lower sideband modes linearly grow to a high saturation level. Then the primary Langmuir mode is amplified and strongly modulated through interaction with the sideband modes. © *2006 American Institute of Physics*. [DOI: 10.1063/1.2348088]

I. INTRODUCTION

Generation of electron plasma waves during an electron beam-plasma interaction is one of the most fundamental processes in plasmas. Strongly modulated waveforms and wave packets of Langmuir waves were commonly observed by spacecrafts in the auroral ionosphere,[1–4] the solar wind,[5–7] the electron foreshock region,[8–10] and the magnetotail.[11] The amplitude-modulated Langmuir waves were also observed in self-consistent kinetic simulations of electron beam instabilities.[12–17]

Several theories were adopted to explain mechanisms for the amplitude modulation of Langmuir waves. The first is the modulational instability, i.e., four-wave interaction.[12,18,19] However, electron beam-driven Langmuir wave packets observed in the magnetosphere lie well outside the region of parameter space for which the modulational instability can proceed.[22]

The second is the parametric decay of the Langmuir wave into ion acoustic waves[16,20–22] or lower hybrid waves.[1–4] In these processes the amplitude of primary Langmuir waves must be high enough to modulate ion distributions. The observations in the magnetosphere showed that the amplitude of Langmuir waves packets sometimes exceeded several hundred mV/m.[1–4,16] On the other hand, the GEOTAIL spacecraft observation in the magnetotail showed the amplitude of fundamental Langmuir waves was several hundred μV/m,[11] which cannot be explained by the Langmuir decay instability.

Another possible mechanism for the amplitude modulation is the "kinetic localization."[13,14] Recently this mechanism developed into the nonlinear trapping theory.[15,17] In this new theory, the amplitude modulation is examined as a result of nonlinear interaction between the excited electrostatic waves and electrons trapped in the electrostatic potential wells. The nonlinear trapping theory gives the spatial length of modulation as $L_M = 2\pi v_p/\omega_b$, where v_p represents the phase velocity of the primary Langmuir mode and $\omega_b \equiv \sqrt{ek_L|E_x(k_L)|/m_e}$ represents the bounce frequency of electrons trapped in the electrostatic potential of the primary Langmuir mode. Here, e, m_e, k_L, and $|E_x(k_L)|$ denote electron charge, mass of electron, wave number of the primary Langmuir mode, and the wave amplitude of the primary Langmuir mode, respectively. The waveforms of amplitude-modulated Langmuir waves obtained by the recent computer simulations were quite similar to the waveforms of Langmuir wave packets observed by the GEOTAIL spacecraft. The simulated spatial length of modulation was roughly estimated as $L_M/2 < L_{\text{simulation}} < L_M$.[17]

To understand detailed mechanisms for the amplitude modulation of Langmuir waves by other processes occurring in weak-electron-beam instabilities, we performed kinetic simulations. In contrast to the previous Particle-In-Cell (PIC) simulations, we used a one-dimensional electrostatic Vlasov simulation technique, in which the numerical noise level is much lower than that in PIC simulations.

The paper is structured as follows: First, the numerical schemes, the simulation model, and the parameters used in the present study are introduced in Sec. II. Second, the full details of the Vlasov simulation results are discussed in Sec. III. Then, conclusion and discussions are presented in Sec. IV.

II. MODEL AND PARAMETERS

The present one-dimensional Vlasov code uses a third-order conservative interpolation scheme.[23] The simulation domain is taken along an ambient magnetic field. We assume two electron components; A very weak electron beam is drifting against the background major electrons. The density ratio of the beam component $R = n_b/(n_e + n_b)$ is set as 0.1%, where the subscripts "b" and "e" represent beam electrons and background electrons, respectively. We assume that the beam and background electrons have the equal thermal velocity $V_t \equiv V_{te} = V_{tb} = 1.0$. The total electron plasma frequency is assumed as $\omega_{pe} = 1.0$. The beam drift velocity V_d is set as $8.0V_t$. The number of cells is $N_x = 8192$ in the x direction and is $N_{v_x} = 2048$ in the v_x direction over a velocity range from $v_{\max} = 20.0V_t$ to $v_{\min} = -12.0V_t$. The grid spacing is equal to $\Delta x = 0.4\lambda_e$ ($\lambda_e \equiv V_t/\omega_{pe}$), and the time step is equal to

[a)]Electronic mail: umeda@stelab.nagoya-u.ac.jp

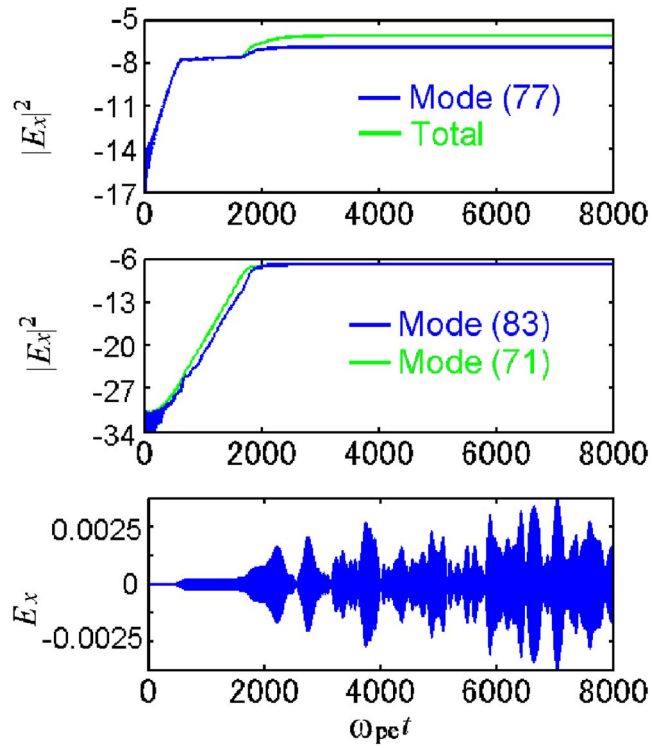

FIG. 1. (Color online) Temporal evolution of the weak-beam instability for the case with a single-mode perturbation. (Top) Energy histories of the total electric field and the primary Langmuir modes ($k_L=77\cdot 2\pi/N_x\Delta x \simeq 0.1476V_t/\omega_{pe}$). (Middle) Energy histories of two sideband modes $k_l=71\cdot 2\pi/N_x\Delta x\simeq 0.1361V_t/\omega_{pe}$ and $k_u=83\cdot 2\pi/N_x\Delta x\simeq 0.1592V_t/\omega_{pe}$. (Bottom) The temporal waveform of the electric field at $x/\lambda_e=0$. The amplitude and wave power of the electric field are normalized by $m_e\omega_{pe}V_t/e$ and $(m_e\omega_{pe}V_t/e)^2=n_eT_e$, respectively. The mode number represents the number of spatial oscillation cycles in the x direction.

$\omega_{pe}\Delta t=0.005$. In the x direction we imposed the periodic boundary condition. In the v_x direction we imposed the open boundary condition where constant numerical fluxes $v_{\max}f(v_{\max})$ and $v_{\min}f(v_{\min})$ are assumed while outgoing perturbations of distribution functions are perfectly absorbed.

In the present study we did not consider ion dynamics, because the amplitude modulation of Langmuir waves can occur without ion dynamics in weak-electron-beam instabilities.[17] This assumption is needed to exclude the amplitude modulation by modulational or decay instabilities in which ion mode waves are involved. We also imposed a single wave mode perturbation only at the most unstable wave number $k_L=77\cdot 2\pi/N_x\Delta x\simeq 0.1476V_t/\omega_{pe}$. This is also needed to neglect the effect of initial thermal fluctuations. In the previous PIC simulations, there appeared electron bunches in the velocity-versus-position phase space at the end of the linear stage.[15,17] However, the pattern of the electron bunches was strongly affected by "enhanced" initial thermal fluctuations of PIC simulations. Note that we need a seed perturbation at the outset of a Vlasov simulation. The numerical procedure for the initialization is described in Ref. 24. Later we also imposed a white noise as the initial perturbation to see the effect of the initial perturbation.

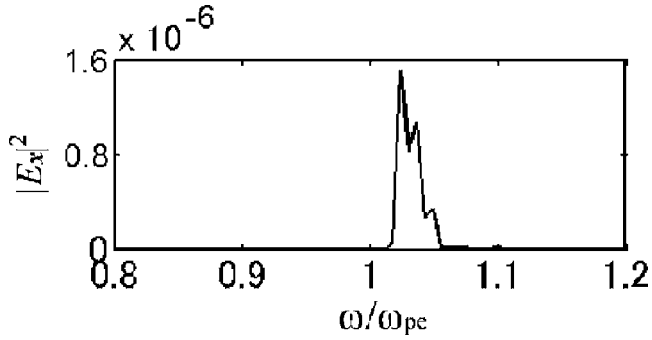

FIG. 2. Frequency spectrum obtained by Fourier transformation of the electric field data for $\omega_{pe}t=7000-8000$. The wave power is normalized by $(m_e\omega_{pe}V_t/e)^2=n_eT_e$.

III. SIMULATION RESULTS

A. Excitation of primary and sideband modes

Figure 1 shows the temporal evolution of the weak-beam instability. In the top panel we plot energy histories of the total electric field and the primary Langmuir modes ($k_L=77\cdot 2\pi/N_x\Delta x\simeq 0.1476V_t/\omega_{pe}$). The middle panel shows energy histories of two sideband modes $k_l=71\cdot 2\pi/N_x\Delta x \simeq 0.1361V_t/\omega_{pe}$ and $k_u=83\cdot 2\pi/N_x\Delta x\simeq 0.1592V_t/\omega_{pe}$. The bottom panel shows the temporal waveform of the electric field at $x/\lambda_e=0$. The electric field is normalized by $\sqrt{n_eT_e}=\sqrt{n_em_eV_t^2}=m_e\omega_{pe}V_t/e$.

The primary Langmuir mode grows from the imposed seed perturbation ($|E_x|^2\sim 10^{-14}n_eT_e$), while other modes grow from the minimum noise level of the double-precision numerical computation ($\sim 10^{-30}$). The total energy of the electric field is contributed only by the primary Langmuir mode until $\omega_{pe}t\sim 1800$, because sideband modes around k_L saturate at a very low level with the saturation of the primary Langmuir mode. On the other hand, the energy histories of the two sideband modes (71) and (83) show that they did grow at almost the same growth rate to a level higher than the saturation level of the primary Langmuir mode. Note that the saturation level of the primary Langmuir mode is $|E_x|^2\sim 10^{-5}n_eT_e$.

When the amplitude of the sideband modes becomes higher than the saturation level of the primary Langmuir mode, the primary Langmuir mode is amplified by interaction with these sideband modes. Then the waveform shows a strong modulation. There also appears apparent difference between the energies of total electric field and the primary Langmuir mode, implying that the modulated waveform consists of many wave modes.

Figure 2 shows the frequency spectrum obtained by Fourier transformation of the electric field data for $\omega_{pe}t=7000-8000$. The amplitude-modulated Langmuir waves have a broader frequency spectrum, showing several discrete spectrum components at frequencies higher than the electron plasma frequency. The frequency spectrum (Fig. 2) and waveform (Fig. 1) of the amplitude-modulated Langmuir waves after the saturation of the sideband modes are very similar to those observed by the GEOTAIL spacecraft.[11,17]

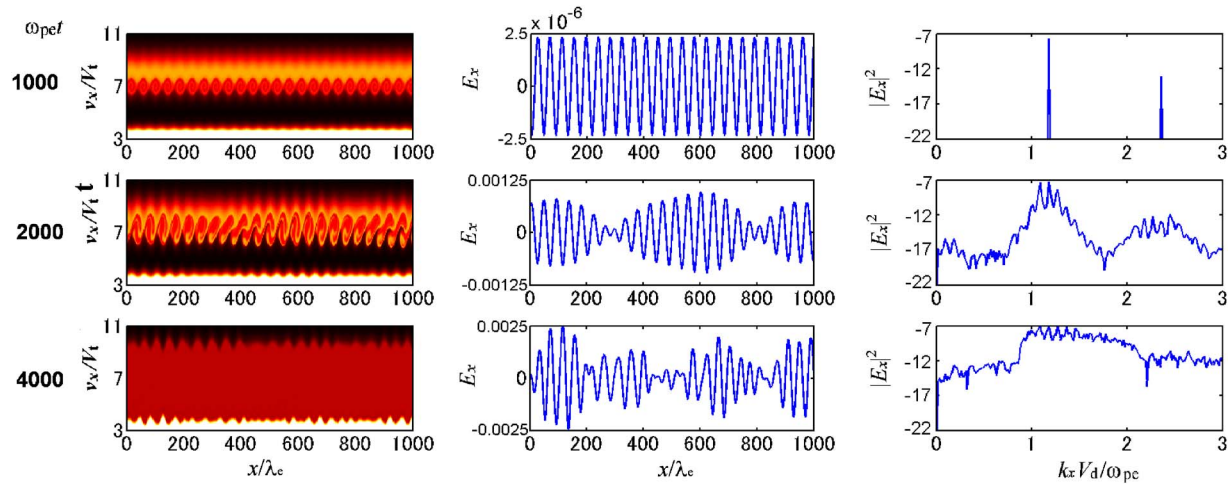

FIG. 3. (Color online) (Left) Velocity versus position phase-space distribution functions at $\omega_{pe}t=1000$, 2000, and 4000. (Middle) The corresponding spatial waveforms, and (left) the wave power spectra $|E_x|^2$ versus wave number. The amplitude and wave power of the electric field are normalized by $m_e\omega_{pe}V_t/e$ and $(m_e\omega_{pe}V_t/e)^2=n_eT_e$, respectively.

B. Amplitude modulation processes

Figure 3 shows correlation between electron trapping phenomenon in velocity versus position phase space and spatial modulation of the electric field. In the left panels we plot x-v_x phase-space diagrams at $\omega_{pe}t=1000$, 2000, and 4000. In the middle and right panels we plotted the corresponding spatial profiles of the electric field and their wave number spectra, respectively.

The time $\omega_{pe}t=1000$ corresponds to the saturation stage of the primary Langmuir mode, in which we found the sinusoidal waveform and the corresponding uniform phase-space vortices. We also found the generation of harmonics Langmuir modes,[24–26] but this is not focused on in this paper.

At $\omega_{pe}t=2000$, there appear electron bunches in the phase space. These bunches due to electron trapping takes place in association with the coherent spatial modulation of the electric field in this stage.[15,17] The power spectrum shows several peaks with a wave number interval of $\Delta k_L=6\cdot 2\pi/N_x\Delta x=0.0115V_t/\omega_{pe}$. This result suggests that the spatial modulation is not due to a wave mode with a long wavelength but due to sideband modes with the wave number difference of Δk_L.

In the present simulation result, the frequency and wave number of the primary Langmuir mode are $\omega_L/\omega_{pe}=1.024$ and $k_LV_d/\omega_{pe}=1.181$, respectively. The saturated amplitude of the primary Langmuir mode is $|E_x|\simeq 2.0\times 10^{-3}n_em_eV_t^2/e$. Thus the phase velocity and bounce frequency are given as $v_p/V_d=0.8671$ and $\omega_b/\omega_{pe}=0.0486$, respectively. With these quantities we obtained the spatial length of modulation as $L_M/\lambda_e\simeq 896.77$, the wave number of which corresponds to $\Delta k_M\simeq 3.654\cdot 2\pi/N_x\Delta x$. The spatial length of modulation in the present simulation result at $\omega_{pe}t=2000$ is shorter than that obtained based on the nonlinear trapping theory.[17] However, the generation of upper and lower sideband modes cannot be explained by the nonlinear trapping theory. The trapping velocity of the primary Langmuir mode in the saturation stage is given as $v_T\equiv 2\omega_b/k_L=0.0823V_d$. Thus wave modes with phase velocities $\omega_L/k_L-v_T\leqslant v_p\leqslant\omega_L/k_L+v_T$ are stabilized by the saturation of the primary Langmuir mode. On the other hand, wave modes with phase velocities outside this range continue to grow even after the saturation of the primary Langmuir mode. The wave numbers at the upper and lower limits of phase velocity are computed as

$$\frac{\omega}{v_p}\simeq\frac{\omega_L}{\omega_L/k_L+v_T}\sim 1.0786V_d/\omega_{pe}$$

and

$$\frac{\omega}{v_p}\simeq\frac{\omega_L}{\omega_L/k_L-v_T}\sim 1.3048V_d/\omega_{pe}.$$

These values are almost equal to the wave numbers of lower and upper sideband modes. Thus the generation of the upper and lower sideband modes and the coherent modulation of primary Langmuir mode in the saturation stage are because Langmuir waves are excited over a wide wave number range by the electron beam instability but the linearly unstable modes are "filtered" by the nonlinear trapping. The sideband modes with wave numbers $k_L-\Delta k_L\leqslant k_x\leqslant k_L+\Delta k_L$ are stabilized by the saturation of the primary Langmuir mode. The difference in wave number between the primary Langmuir mode and its sidebands can be analytically estimated as

$$\Delta k_L=k_L-\frac{\omega_L}{\omega_L/k_L+v_T}\simeq 2\frac{\omega_b}{\omega_L}k_L=2\frac{\omega_b}{v_p},\tag{1}$$

which corresponds to the lower limit of the spatial length of modulation obtained by the previous theory.[17]

In the saturation stage of the sideband modes, $\omega_{pe}t=4000$, we found a strong spatial modulation of electric field. The wave energies of the upper and lower sideband modes exceed the wave energy of the primary Langmuir mode. Then the wave energy of the primary Langmuir mode is amplified to a one-order higher value. Finally there appear spatial Langmuir wave packets. The envelope of the Langmuir wave packets propagates at the group velocity of Langmuir waves which is slower than their phase velocities. The

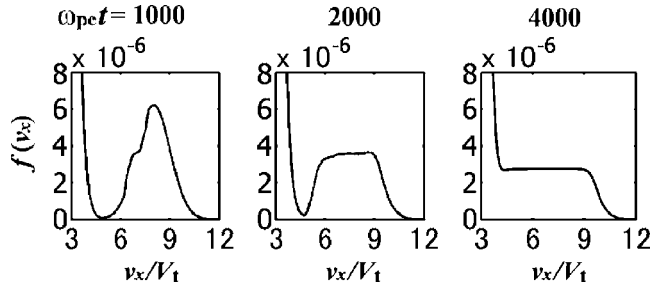

FIG. 4. Electron velocity distribution functions averaged over x at $\omega_{pe}t=1000$, 2000, and 4000.

stable propagation of envelope is observed as the strong amplitude modulation in temporal waveforms. The wave number spectrum shows a turbulent feature by the interaction between the primary Langmuir mode and its upper and lower sidebands. The turbulent feature suggests that wave packets consist of Langmuir waves with various wave numbers but different phases. The phase-space plot also does not show any coherent structure in the turbulent stage, which suggests that the electron bunches in the phase space seen in the saturation stage of the primary Langmuir mode are not the strong spatial amplitude modulation itself in this highly nonlinear stage but are a source of it.

C. Evolution of the velocity distribution function

To study a mechanism for the amplification of the primary Langmuir mode by interaction with the sideband modes, we show averaged velocity distribution functions at $\omega_{pe}t=1000$, 2000, and 4000 in Fig. 4. In the saturation stage of the primary Langmuir mode ($\omega_{pe}t=1000$) we found the formation of a plateau over the trapping velocity range $\omega_L/k_L-v_T \leqslant v_x \leqslant \omega_L/k_L+v_T$. However, this velocity distribution function is still unstable, and thus the upper and lower sideband modes can grow linearly. At $\omega_{pe}t=2000$, the velocity distribution function is modified by the nonlinear trapping due to the upper and lower sideband modes, and at the velocity distribution function there appears to be a positive gentle slope over a wide velocity range, which makes the primary Langmuir mode unstable again. At $\omega_{pe}t=4000$, we found the formation of a plateau over a wide velocity range and there is no further excitation of electrostatic waves. We conclude that the amplification of the primary Langmuir mode and the formation of wave packets are because of this quasilinear-type modification of the velocity distribution function.

D. Effect of initial perturbation

We applied a single mode initial perturbation in the present simulation, which is not realistic. We performed another simulation run with a white noise. Figure 5 shows the temporal evolution of this run. The energy histories and temporal waveform are presented in the same format as the data shown in Fig. 1.

All the wave modes grow from the imposed seed perturbation ($|E_x|^2 \sim 10^{-14}$), but at different growth rates. The primary Langmuir mode quickly saturates earlier because this

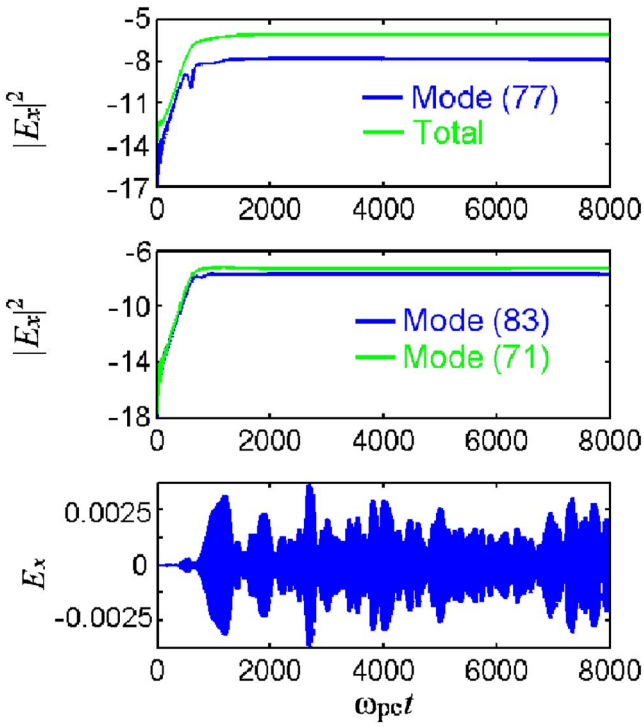

FIG. 5. (Color online) Temporal evolution of the weak-beam instability for the case with a white noise. (Top) Energy histories of the total electric field and the primary Langmuir modes ($k_L=77\cdot 2\pi/N_x\Delta x \simeq 0.1476V_t/\omega_{pe}$). (Middle) Energy histories of two sideband modes $k_l=71\cdot 2\pi/N_x\Delta x \simeq 0.1361V_t/\omega_{pe}$ and $k_u=83\cdot 2\pi/N_x\Delta x \simeq 0.1592V_t/\omega_{pe}$. (Bottom) The temporal waveform of the electric field at $x/\lambda_e=0$. The amplitude and wave power of the electric field are normalized by $m_e\omega_{pe}V_t/e$ and $(m_e\omega_{pe}V_t/e)^2=n_eT_e$, respectively. The mode number represents the number of spatial oscillation cycles in the x direction.

has the maximum growth rate. However, the saturation level of the primary Langmuir mode becomes much lower than the previous case, because sideband modes around k_L saturate at a level much higher than in the previous run with a single-mode perturbation. The energy histories of the two sideband modes (71) and (83) shows that they continue to grow linearly even after the saturation of the primary Langmuir mode, as seen in the previous run. The primary mode again becomes unstable because of the phase-space mixing by interaction between the primary and sideband modes. There appear to be electron bunches in the phase space in the linear stage, not in the saturation stage as seen in the previous run.

In summary, the mechanism for the amplitude modulation in the run with a white noise is the same as that in the run with a single mode perturbation. However, the amplitude of the Langmuir mode is modulated in a much earlier stage. Note that these results are consistent with the previous PIC simulation result by Usui *et al.*[17]

IV. CONCLUSION AND DISCUSSIONS

We performed one-dimensional electrostatic Vlasov simulations of a weak-electron-beam instability and found that Langmuir wave packets were generated by two processes without ion dynamics. The first is the nonlinear trapping filter, by which *linearly unstable* upper and lower sideband modes are enhanced at specific wave numbers. The

second is the nonlinear velocity-space interaction between the primary Langmuir mode and its upper and lower sideband modes. The saturated primary Langmuir mode is again amplified by the modification of the velocity distribution function. The temporal amplitude modulation and packets of Langmuir wave are observed as the result of the spatial modulation propagating at the group velocity.

It is noted that we also performed another simulation run with ion dynamics. However, the temporal evolution of the weak-beam instability and the generation processes of Langmuir wave packets were almost the same as those found in the run without ion dynamics. This is because the amplitude of excited Langmuir waves is too small for Langmuir decay instabilities to occur.

The generation of Langmuir wave packets by Langmuir decay instabilities (e.g., Refs. 10 and 16) are not focused in this paper. In these processes involving ion modes, the wave field energy must be of the order of electron thermal energy. Thus simulations of such a strong-beam instability are left as a future study. However, the amplitude modulation of Langmuir waves studied in this paper includes both cascading and inverse-cascading processes, which would play an important role in the generation of Langmuir turbulence.

ACKNOWLEDGMENTS

The author is grateful to T. Ogino for discussions. The computer simulations were performed on the AKDK supercomputer system at the Research Institute for Sustainable Humanosphere, Kyoto University as a collaborative research project.

[1] R. E. Ergun, C. W. Carlson, J. P. McFadden, J. H. Clemmons, and M. H. Boehm, Geophys. Res. Lett. **18**, 1177 (1991).
[2] K. Stasiewicz, B. Holback, V. Krasnoselskikh, M. Boehm, R. Bostrom, and P. M. Kintner, J. Geophys. Res. **101**, 21515 (1996).
[3] J. Bonnell, P. Kintner, J.-E. Wahlund, and J. A. Holtet, J. Geophys. Res. **102**, 17233 (1997).
[4] G. V. Lizunov, Y. Khotyaintsev, and K. Stasiewicz, J. Geophys. Res. **106**, 24755 (2001).
[5] D. A. Gurnett, G. V. Hospodarsky, W. S. Kurth, D. J. Williams, and S. J. Bolton, J. Geophys. Res. **98**, 5631 (1993).
[6] S. D. Bale, D. Burgess, P. J. Kellogg, K. Goetz, R. L. Howard, and S. J. Monson, Geophys. Res. Lett. **23**, 109 (1996).
[7] P. J. Kellogg, K. Goetz, S. J. Monson, and S. D. Bale, J. Geophys. Res. **104**, 17069 (1999).
[8] P. J. Kellogg, S. J. Monson, K. Goetz, R. L. Howard, J. L. Bougeret, and M. L. Kaiser, Geophys. Res. Lett. **23**, 1243 (1996).
[9] P. J. Kellogg, K. Goetz, S. J. Monson, and S. D. Bale, J. Geophys. Res. **104**, 6751 (1999).
[10] J. Soucek, V. Krasnoselskikh, T. Dudok de Wit, J. Pickett, and C. Kletzing, J. Geophys. Res. **110**, A08102 (2005).
[11] H. Kojima, H. Furuya, H. Usui, and H. Matsumoto, Geophys. Res. Lett. **24**, 3049 (1997).
[12] J. G. Wang, G. L. Payne, D. F. DuBois, and H. A. Rose, Phys. Plasmas **2**, 1129 (1995).
[13] L. Muschietti, I. Roth, and R. E. Ergun, J. Geophys. Res. **100**, 17481 (1995).
[14] L. Muschietti, I. Roth, and R. E. Ergun, J. Geophys. Res. **101**, 15605 (1996).
[15] K. Akimoto, Y. Omura, and H. Matsumoto, Phys. Plasmas **3**, 2559 (1996).
[16] S. Matsukiyo, R. A. Treumann, and M. Scholer, J. Geophys. Res. **109**, A06212 (2004).
[17] H. Usui, H. Furuya, H. Kojima, H. Matsumoto, and Y. Omura, J. Geophys. Res. **110**, A06203 (2005).
[18] V. E. Zakharov, Sov. Phys. JETP **35**, 908 (1972).
[19] P. A. Robinson, Rev. Mod. Phys. **69**, 507 (1997).
[20] I. H. Cairns and P. A. Robinson, Geophys. Res. Lett. **19**, 2187 (1992).
[21] P. A. Robinson and I. H. Cairns, Geophys. Res. Lett. **22**, 2657 (1995).
[22] I. H. Cairns, P. A. Robinson, and N. I. Smith, J. Geophys. Res. **103**, 287 (1998).
[23] T. Umeda, M. Ahsour-Abdalla, and D. Schriver, "Comparison of numerical interpolation schemes for one-dimensional electrostatic Vlasov code," J. Plasma Phys. (to be published).
[24] T. Umeda, Y. Omura, P. H. Yoon, R. Gaelzer, and H. Matsumoto, Phys. Plasmas **10**, 382 (2003).
[25] P. H. Yoon, R. Gaelzer, T. Umeda, Y. Omura, and H. Matsumoto, Phys. Plasmas **10**, 364 (2003).
[26] R. Gaelzer, P. H. Yoon, T. Umeda, Y. Omura, and H. Matsumoto, Phys. Plasmas **10**, 373 (2003).